Applied Catalysis B: Environmental 324 (2023) 122266

Contents lists available at ScienceDirect

Applied Catalysis B: Environmental

journal homepage: www.elsevier.com/locate/apcatb

Degradation of organic compounds through both radical and nonradical activation of peroxymonosulfate using $CoWO_4$ catalysts

Anh Quoc Khuong Nguyen [a], Yong-Yoon Ahn [b], Gwanyong Shin [c], Younsang Cho [d], Jonghun Lim [d], Kitae Kim [b], Jungwon Kim [c,*]

[a] Department of Chemistry, Hallym University, Chuncheon, Gangwon-do 24252, Republic of Korea
[b] Korea Polar Research Institute (KOPRI), Incheon 21990, Republic of Korea
[c] Department of Environmental Sciences and Biotechnology, Hallym University, Chuncheon, Gangwon-do 24252, Republic of Korea
[d] Department of Environment and Energy Engineering, Sungshin Women's University, Seoul 01133, Republic of Korea

ARTICLE INFO

Keywords:
Cobalt tungstate
Peroxymonosulfate activation
Sulfate radical
Nonradical mechanism
Aqueous organic compounds

ABSTRACT

In this study, we synthesized high-efficiency stable $CoWO_4$ nanoparticles that can be used as peroxymonosulfate (PMS) activators for water treatment by adjusting the pH during hydrothermal synthesis. The $CoWO_4$ catalyst synthesized at pH 10 ($CoWO_4$_10), which had the largest surface area and the best charge transfer characteristics, showed the highest degradation efficiency for 4-chlorophenol and the highest stability for metal ion leaching. The first-order degradation rate constant was 10.9 min^{-1}, and the Co and W leaching concentrations after 1 h of catalytic reaction were 1.1 and 4.2 μM, respectively. All the 16 tested organic compounds were rapidly degraded. The degradation performance of $CoWO_4$_10 was 2.4−83.6 times better than those of other Co-based metal oxides. In this regard, the $CoWO_4$_10 can be considered a practical PMS activator. This study provides a simple strategy for the development of highly efficient and stable bimetallic oxides that can be utilized in various fields.

1. Introduction

Peroxymonosulfate (PMS, HSO_5^-) has been extensively used for the oxidative degradation of organic compounds in water because of its economic efficiency and eco-friendliness [1,2]. PMS can be directly employed as an oxidant to degrade specific organic compounds such as trimethoprim [3], tetracycline [4], methyl parathion [5], and *p*-aminobenzoic acid [6]. However, this system generally shows low degradation efficiency (i.e., the complete degradation of parent compounds takes a long time (a few hours) at millimolar levels of PMS) and, in particular, limited mineralization efficiency [7,8]. PMS is frequently activated using various methods to enhance the degradation and mineralization efficiency. PMS activation can be classified into two categories: radical and nonradical. Energy (e.g., heat [9], ultrasound [10], and UV-C [11]) and electrons (i.e., reductants such as hydroxylamine [12], ascorbic acid [13], and zero-valent zinc [14]) induce the homolytic and heterolytic cleavage of PMS, respectively, to produce highly reactive hydroxyl ($^{\bullet}OH$) and sulfate radicals ($SO_4^{\bullet-}$). In contrast, the presence of electron mediators (e.g., graphitized nanodiamonds [15], carbon nanotubes [16], and noble metal nanoparticles [17]) can accelerate electron transfer from organic compounds to PMS, resulting in more rapid degradation without producing radical species.

Transition metal ions, such as Cu^{2+} [18], Fe^{2+} [19], and Co^{2+} [20], have been employed as homogeneous reductants to induce radical activation of PMS. Among the various transition metal ions (Co^{2+}, Cu^{2+}, Ni^{2+}, Fe^{2+}, Fe^{3+}, Ru^{3+}, Ce^{3+}, V^{3+}, Mn^{2+}, and Ag^{+}), Co^{2+} shows the highest activity for the degradation of aqueous organic compounds through PMS activation [21,22]. However, the use of homogeneous Co^{2+} as a PMS activator requires the continuous addition of Co^{2+} and a post-separation process to remove Co ions remaining in the treated water. Therefore, Co-based heterogeneous catalysts have been considered as alternative solutions.

Monometallic oxides such as CoO and Co_3O_4 were first introduced as heterogeneous PMS activators [23]. However, they suffer from low stability related to Co ion leaching or low activity for PMS activation [24–26]. Bimetallic oxides usually exhibit higher catalytic performance for PMS activation and stability toward Co ion leaching than monometallic oxides. The higher electrical conductivity of bimetallic oxides provides favorable conditions for electron transfer from metal ions on the surface to PMS, resulting in the production of more radical species

* Corresponding author.
E-mail address: jwk@hallym.ac.kr (J. Kim).

https://doi.org/10.1016/j.apcatb.2022.122266
Received 22 September 2022; Received in revised form 2 December 2022; Accepted 4 December 2022
Available online 6 December 2022

[27,28]. The strong interaction between Co and the other metal (Co−O−M) in bimetallic oxides diminishes the dissolution of Co ions in water [29,30]. In addition, electron transfer between the redox couple of Co^{2+}/Co^{3+} and $M^{x+}/M^{(x+1)+}$ in bimetallic oxides enhances the regeneration of Co^{2+}, which maintains the catalytic activity for PMS activation [31,32]. In this regard, a variety of bimetallic oxides comprising Co and other metals in their structure, such as $CoFe_2O_4$ [33], $CoMn_2O_4$ [34], $CuCo_2O_4$ [35], $NiCo_2O_4$ [36], and $LaCoO_3$ [37], have been fabricated and used for the degradation of organic compounds in the presence of PMS. Despite significant efforts, developing more efficient and stable PMS activators for water treatment remains challenging.

Cobalt tungstate ($CoWO_4$) has been employed in various electrochemical systems, such as sensors [38], supercapacitors [39], water splitting [40], fuel cells [41], and solar cells [42], owing to the aforementioned advantages of the incorporation of W atoms into cobalt oxides. Although a variety of $CoWO_4$-based composites, such as $Bi_2WO_6/CoWO_4$ [43], $ZnWO_4/CoWO_4$ [44], $CdS/CoWO_4$ [45], $g\text{-}C_3N_4/CoWO_4$ [46], $SrTiO_3/Ag_2S/CoWO_4$ [47], and $Ag_3PO_4/CoWO_4$ [48], have been used as photocatalysts or sonocatalysts for the degradation of organic compounds, $CoWO_4$ has not been used as a PMS activator in environmental remediation. All the previously reported $CoWO_4$-based composites require external energy (light or ultrasound). However, the $CoWO_4$/PMS system can operate in the dark without external energy. In addition, the material cost of $CoWO_4$ is lower than those of the $CoWO_4$-based composites.

In this study, we synthesized $CoWO_4$ nanoparticles using a hydrothermal method under various pH conditions and used them as PMS activators for the degradation of organic compounds. Based on the catalytic activity for PMS activation (i.e., degradation efficiency of 4-chlorophenol) and stability (i.e., leaching concentrations of Co and W ions), the best $CoWO_4$ was determined. $CoWO_4$ was characterized using various analytical methods and its degradation mechanism was systematically investigated. The effects of the reaction parameters and background species on the degradation kinetics were investigated and discussed. In addition, the practical viability of $CoWO_4$ as a PMS activator for water treatment was evaluated in terms of its reusability, relative activity compared to other Co-based metal oxides, and applicability to diverse organic compounds.

2. Experimental

2.1. Chemicals and materials

The chemicals and materials were used as received without further purification. They include the following: potassium peroxymonosulfate ($KHSO_5{\cdot}0.5KHSO_4{\cdot}0.5K_2SO_4$), cobalt(II) chloride hexahydrate ($CoCl_2{\cdot}6H_2O$), sodium tungstate dihydrate ($Na_2WO_4{\cdot}2H_2O$), methanol (CH_3OH), *tert*-butyl alcohol ($(CH_3)_3COH$), ethanol (C_2H_5OH), sodium hydroxide (NaOH), boric acid (H_3BO_3), hydrochloric acid (HCl), phenol (C_6H_5OH), 2-chlorophenol (ClC_6H_4OH), 2-nitrophenol ($O_2NC_6H_4OH$), 4-chlorophenol (ClC_6H_4OH), 4-nitrophenol ($O_2NC_6H_4OH$), 4-bromophenol (BrC_6H_4OH), 4-methylphenol ($CH_3C_6H_4OH$), 2,4-dimethylphenol ($(CH_3)_2C_6H_3OH$), 2,4-dichlorophenol ($Cl_2C_6H_3OH$), bisphenol A ($(CH_3)_2C(C_6H_4OH)_2$), propranolol hydrochloride ($C_{16}H_{21}NO_2{\cdot}HCl$), sulfamethoxazole ($C_{10}H_{11}N_3O_3S$), sulfisoxazole ($C_{11}H_{13}N_3O_3S$), sulfanilamide ($H_2NC_6H_4SO_2NH_2$), cimetidine ($C_{10}H_{16}N_6S$), ranitidine hydrochloride ($C_{13}H_{22}N_4O_3S{\cdot}HCl$), polyethylene glycol ($H(OCH_2CH_2)_nOH$), 5-*tert*-butoxycarbonyl-5-methyl-1-pyrroline-*N*-oxide ($C_{10}H_{17}NO_3$), ammonium acetate ($CH_3CO_2NH_4$), methanesulfonic acid (CH_3SO_3H), phosphoric acid (H_3PO_4), acetonitrile (CH_3CN), sodium perchlorate ($NaClO_4$), sodium phosphate (Na_3PO_4), sodium bicarbonate ($NaHCO_3$), sodium carbonate (Na_2CO_3), sodium chloride (NaCl), sodium nitrate ($NaNO_3$), potassium iodide (KI), deuterium oxide (D_2O), humic acid, nitrogen gas (N_2), fluorine-doped tin oxide coated glass (FTO glass), cobalt(II, III) oxide (Co_3O_4), cobalt(II) oxide (CoO), cobalt tungstate ($CoWO_4$), cobalt aluminum oxide ($CoAl_2O_4$), cobalt iron oxide ($CoFe_2O_4$), and lithium cobalt(III) oxide ($LiCoO_2$). The specific information about the chemicals and materials used is detailed in Table S1. All solutions and suspensions were prepared in deionized water (resistivity ≈ 18.3 MΩ·cm), which was produced using a water purification system (Millipore Milli-Q Direct 8).

2.2. Synthesis and characterization of $CoWO_4$ nanoparticles

Bimetallic $CoWO_4$ nanoparticles were prepared via a hydrothermal method using cobalt(II) chloride hexahydrate and sodium tungstate dihydrate as Co and W precursors, respectively. The synthesis procedure is illustrated in Fig. S1. First, sodium tungstate dihydrate solution (2.31 g/35 mL, 0.2 M) was added dropwise to the cobalt(II) chloride hexahydrate solution (1.67 g/35 mL, 0.2 M) under vigorous magnetic stirring. The pH of the mixture was adjusted to the desired values (6−10) using HCl (12 M) or NaOH (10 M) solutions. After 10 min, the mixture was transferred into a 100 mL Teflon-lined autoclave (iNexus IN-HT100), which was then placed in an electric oven (Daihan Scientific WON-32) at 200 °C for 24 h. The $CoWO_4$ powder was collected via vacuum filtration, washed with deionized water, and calcined in a furnace (Daihan Scientific FHX-12) at 700 °C for 3 h. The obtained samples were denoted as $CoWO_4$_x, where x represents the pH of the mixture during the synthesis process. The color of the $CoWO_4$ powders was markedly different depending on the synthetic pH (blue for $CoWO_4$_6, dark blue for $CoWO_4$_7, gray for $CoWO_4$_8, black for $CoWO_4$_9, and black for $CoWO_4$_10; Fig. S2). $CoWO_4$_10 was used in the degradation experiments unless otherwise stated. Monometallic Co_3O_4 was synthesized in the same way as $CoWO_4$ at pH 10 without the addition of a sodium tungstate dihydrate solution.

The crystal structures of the $CoWO_4$ samples were identified using X-ray diffraction (XRD, Malvern Panalytical X′Pert Pro MPD). The morphology and elemental distribution of $CoWO_4$ were investigated using a field-emission transmission electron microscope (FE-TEM, JEOL JEM-2100F) equipped with an energy-dispersive X-ray (EDX) spectrometer. The Brunauer-Emmett-Teller (BET) surface areas and pore volumes of the $CoWO_4$ were measured using a gas sorption analyzer (Quantachrome Instruments Quadrasorb evo). The chemical states of Co, W, and O on the surface of $CoWO_4$ were determined using X-ray photoelectron spectroscopy (XPS, Thermo Scientific K-Alpha). The detailed operating parameters for the characterization of $CoWO_4$ are listed in Table S2.

The $CoWO_4$ electrodes were prepared using the doctor blade method [49]. Electrochemical measurements were performed using a computer-controlled potentiostat (Biologic VSP-300) with the $CoWO_4$ electrode (working electrode), a platinum sheet (counter electrode), and a Ag/AgCl electrode (reference electrode). $NaClO_4$ (50 mM) was used as a supporting electrolyte. Details of the preparation of the $CoWO_4$ electrode and the conditions for the electrochemical measurements are described in Text S1.

2.3. Experimental procedure and analytical methods

A certain amount of $CoWO_4$ (or other Co-based metal oxides) was added to the deionized water and sonicated for 1 min. Aliquots of the organic compounds, borate buffer, and PMS stock solutions were sequentially added to the $CoWO_4$ suspension. The initial concentrations of $CoWO_4$, organic compounds, borate buffer, and PMS were 15 mg/30 mL, 100 μM, 50 mM, and 1 mM, respectively, and the pH of the suspension was 8.0. The moment the PMS solution was added was considered the start of the reaction. A 50 mL glass beaker was used as the reactor, which was open to ambient air and stirred magnetically during the catalytic reaction. All reactions were carried out in an aluminum foil-covered box to prevent ambient light-induced photochemical reactions. At predetermined time intervals, sample aliquots were withdrawn from the reactor, filtered through a polytetrafluoroethylene filter (Millipore, 0.45 μm), transferred into a glass vial containing methanol (2 M,

residual radical scavenger), and immediately analyzed. All experiments were performed two or more times, and the results are presented as mean ± standard deviation, except for the electrochemical results.

The concentrations of organic compounds were measured using a high-performance liquid chromatograph (HPLC, Agilent 1220) equipped with a Zorbax 300SB C-18 column (4.6 mm × 150 mm) and a UV−visible detector. The operating parameters for the HPLC analysis are listed in Table S3. Inductively coupled plasma optical emission spectrometry (ICP-OES, Thermo Scientific iCAP 6300) was used to detect the concentrations of Co and W ions leached from the $CoWO_4$ catalysts. The concentration of PMS was determined using an iodometric method [50], in which the oxidation of iodide by PMS produces triiodide ($HSO_5^-(aq) + 3I^-(aq) + H^+(aq) \rightarrow SO_4^{2-}(aq) + I_3^-(aq) + H_2O(l)$) (see Text S2 for details). Electron spin resonance (ESR) analysis to detect radical species was performed using an ESR spectrometer (Bruker EMXnano). 5-*tert*-butoxycarbonyl-5-methyl-1-pyrroline-*N*-oxide (BMPO) was used as the spin-trapping reagent. The operating conditions for the ESR analysis are summarized in Table S4.

3. Results and discussion

3.1. Characterization of $CoWO_4$ catalysts

The synthetic pH during the hydrothermal process can significantly affect the chemical and physical properties of metal oxides [51,52]. Therefore, $CoWO_4$ nanoparticles prepared under different pH conditions were systematically investigated. Fig. 1 shows the XRD patterns of the $CoWO_4$ catalysts synthesized under different pH conditions. The diffraction peaks at 2θ = 15.6°, 19.0°, 23.8°, 24.7°, 30.7°, 31.5°, 36.3°, 38.6°, 41.3°, 44.4°, 45.8°, 48.8°, 50.6°, 52.1°, 54.0°, 61.8°, 63.8°, 65.1°, 68.7°, and 71.8° were observed in all $CoWO_4$ samples ($CoWO_4$_6, $CoWO_4$_7, $CoWO_4$_8, $CoWO_4$_9, and $CoWO_4$_10). These peaks correspond to the (010), (001), (−110), (011), (−111), (020), (200), (002), (−201), (−211), (−112), (−220), (022), (031), (−122), (−311), (222), (−231), (−140), and (−123) crystal planes of monoclinic $CoWO_4$ (JCPDS file No. 15−0867) [53]. As an exception, a small peak at 2θ = 23.1° (*), which was assigned to the (002) planes of monoclinic WO_3 (JCPDS file No. 43−1035) [54], appeared in the $CoWO_4$_6 sample. The reaction between protons and tungstate ions (WO_4^{2-}) under acidic conditions appears to be responsible for the formation of WO_3 ($2H^+(aq) + WO_4^{2-}(aq) \rightarrow WO_3(s) + H_2O(l)$ [55]). These XRD results indicate that the $CoWO_4$ catalysts synthesized above pH 7.0 are pure $CoWO_4$; however, the $CoWO_4$ catalyst synthesized at pH 6.0 is technically a WO_3/$CoWO_4$ composite.

The morphologies of the $CoWO_4$ catalysts synthesized under different pH conditions were investigated and compared using TEM (Fig. 2). $CoWO_4$_6 and $CoWO_4$_7 exhibited nearly spherical appearances (Fig. 2a and b). $CoWO_4$_8 exhibited spherical, oval, and rectangular morphologies (Fig. 2c). However, various morphologies, including

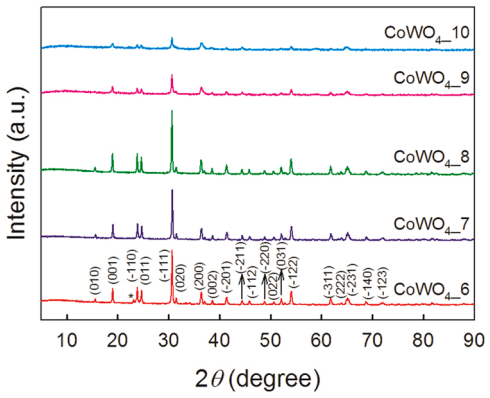

Fig. 1. XRD patterns of $CoWO_4$ catalysts synthesized at different pH conditions.

spherical, oval, rectangular, and shapeless forms, were observed in $CoWO_4$_9 and $CoWO_4$_10, with a wide size distribution ranging from a few nanometers to dozens of nanometers (Fig. 2d and e). Because Co species mainly exist as Co^{2+} under acidic and neutral conditions, the nucleation rate of $CoWO_4$ ($Co^{2+}(aq) + WO_4^{2-}(aq) \rightarrow CoWO_4(s)$ [39]) is fast (i.e., nucleation is more dominant than crystal growth); therefore, the $CoWO_4$ nuclei tend to aggregate and form spherical particles to minimize the surface free energy [56]. Under basic conditions, the concentration of Co^{2+} in the solution decreases owing to its hydrolysis ($Co^{2+}(aq) + H_2O(l) \rightarrow Co(OH)^+(s) + H^+(aq)$ and $Co^{2+}(aq) + 2H_2O(l) \rightarrow Co(OH)_2(s) + 2H^+(aq)$ [57]), which retards the formation of $CoWO_4$ nuclei [58]. In this situation (i.e., crystal growth is more dominant than nucleation), the adsorption of Co^{2+} and WO_4^{2-} ions on specific crystal planes of the $CoWO_4$ nuclei results in various morphologies owing to different crystal growth orientations [59].

The elemental distribution images of the $CoWO_4$ catalysts reveal that the three components (Co, W, and O) overlap. This result confirms that the materials synthesized in this study are composed of Co, W, and O, which are uniformly distributed in the $CoWO_4$ particles.

3.2. Degradation of 4-CP by $CoWO_4$ in the presence of PMS

The degradation kinetics of the organic compounds in the suspension of $CoWO_4$ with PMS (i.e., in the $CoWO_4$/PMS system) were investigated and compared with those in the control systems (Fig. 3). $CoWO_4$ synthesized at pH 10 ($CoWO_4$_10) and 4-chlorophenol (4-CP) were selected as the catalyst and model organic compound, respectively. 4-CP was degraded very rapidly in the presence of both $CoWO_4$ and PMS. After 10 s, 84.2% of the 4-CP was degraded, and the degradation was complete within 1 min. However, the degradation of 4-CP was negligible in the absence of $CoWO_4$ or PMS. These results indicate that $CoWO_4$ can activate PMS to induce the degradation of 4-CP.

The degradation of 4-CP in the $CoWO_4$/PMS system was accompanied by the production of various intermediates such as benzoquinone, hydroxy-1,4-benzoquinone, 4-chlorocatechol, maleic acid, 4-chloro-5-hydroxy-1,2-benzoquinone, 2,5-dihydroxy-1,4-benzoquinone, 2-chloromaleic acid, 2-(4-hydroxyphenyl)-1,4-benzoquinone, 5,5′-dichloro-2,2′-biphenyldiol, and 5-chloro-2,4′-biphenyldiol. The concentrations of most of the intermediates increased during the initial period and then decreased (Fig. S3). Based on the results of the intermediate analysis and previous studies on 4-CP degradation through radical and nonradical mechanisms [60,61], the possible degradation pathways of 4-CP in the $CoWO_4$/PMS system are illustrated in Scheme S1. The removal efficiency of total organic carbon (TOC) was 62.0% after 30 min of reaction (Fig. S4), implying that the intermediates were fully oxidized to CO_2.

3.3. Catalytic activity of $CoWO_4$ catalysts based on the synthetic pH

The catalytic activities of the $CoWO_4$ catalysts in the degradation of 4-CP in the presence of PMS were compared (Fig. 4a). The degradation of 4-CP proceeded more rapidly when $CoWO_4$ was synthesized at higher pH ($CoWO_4$_10 > $CoWO_4$_9 > $CoWO_4$_8 > $CoWO_4$_7 > $CoWO_4$_6). The first-order rate constants for 4-CP degradation (k) were 0.7 min^{-1} for $CoWO_4$_6, 2.0 min^{-1} for $CoWO_4$_7, 8.5 min^{-1} for $CoWO_4$_8, 10.5 min^{-1} for $CoWO_4$_9, and 10.9 min^{-1} for $CoWO_4$_10 (Fig. 4b). The complete degradation of 4-CP was achieved within 1 min for $CoWO_4$_8, $CoWO_4$_9, and $CoWO_4$_10. In contrast, the degradation efficiencies of 4-CP after 1 min on $CoWO_4$_6 and $CoWO_4$_7 were 53.2% and 78.7%, respectively.

The number of active sites on the catalyst surface for PMS activation increases with increasing surface area and pore volume [62,63]. Table 1 lists the BET surface areas and pore volumes of the $CoWO_4$ catalysts depending on the synthetic pH. Both the BET surface area and pore volume increased with increasing pH. The surface area (also pore volume) and crystallinity are generally inversely proportional to each other [64,65]. Therefore, this behavior is consistent with the XRD patterns, which showed lower crystallinity at higher pH. Fig. S5 shows the

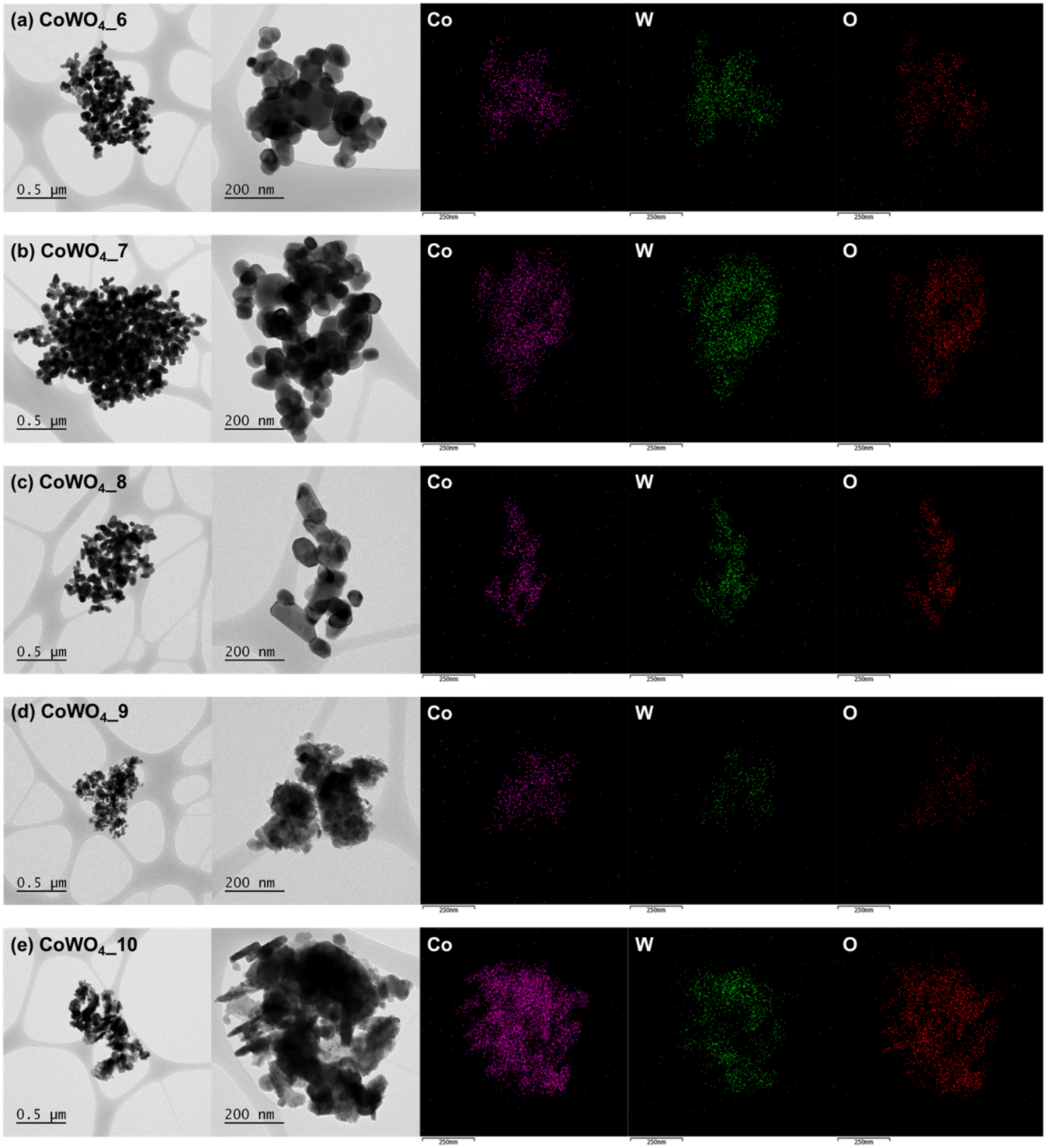

Fig. 2. TEM and elemental distribution images of $CoWO_4$ catalysts synthesized at pH (a) 6, (b) 7, (c) 8, (d) 9, and (e) 10.

hydrodynamic particle size distribution of the $CoWO_4$ catalysts depending on the synthetic pH. The hydrodynamic particle size decreased with increasing pH. Because $CoWO_4$ synthesized at a higher pH has a larger surface area (also pore volume) and smaller hydrodynamic particle size (surface area: $CoWO_4$_10 > $CoWO_4$_9 > $CoWO_4$_8 > $CoWO_4$_7 > $CoWO_4$_6 and average particle size: $CoWO_4$_10 (101 nm) < $CoWO_4$_9 (106 nm) < $CoWO_4$_8 (127 nm) < $CoWO_4$_7 (131 nm) < $CoWO_4$_6 (139 nm)), the catalytic activity appears to increase as the synthetic pH increases.

We investigated the charge-transfer properties of the $CoWO_4$ catalysts using electrochemical analysis (Fig. 5). The arc size in the electrochemical impedance spectroscopy (EIS) Nyquist plot (i.e., electron transfer resistance [66]) was smaller when the synthetic pH was higher (arc size: $CoWO_4$_10 < $CoWO_4$_9 < $CoWO_4$_8 < $CoWO_4$_7) (Fig. 5a). The slope of the Mott-Schottky plot, which is inversely proportional to the charge carrier density [67], decreases with increasing synthetic pH (Fig. 5b). These results confirm that electron transfer in the $CoWO_4$ catalysts synthesized at higher pH values is more efficient. The highest electron transfer efficiency, along with the highest surface area, can help explain why the degradation efficiency of 4-CP in the presence

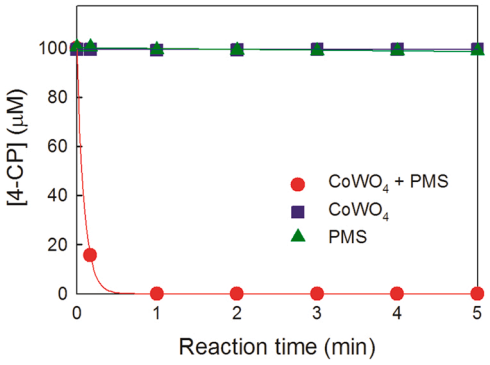

Fig. 3. Time profiles of the 4-CP concentration in the suspension of $CoWO_4$ with PMS and control experiments. Experimental conditions: [$CoWO_4$] = 15 mg/30 mL, [PMS] = 1 mM, [4-CP] = 100 μM, and pH = 8.0.

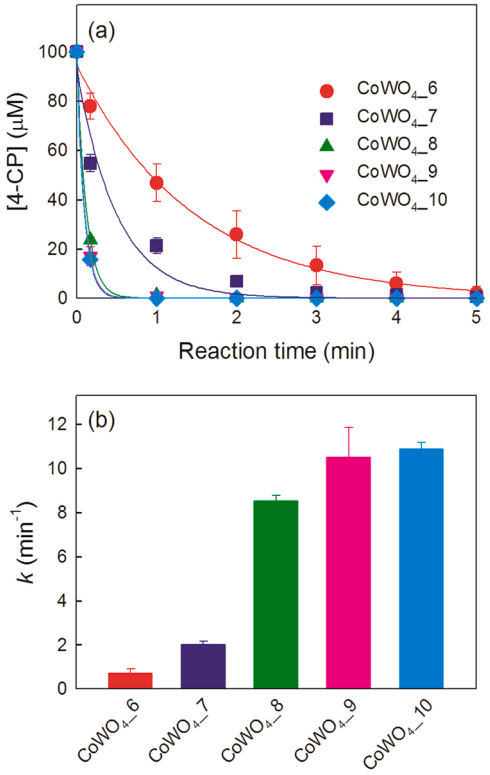

Fig. 4. (a) Time profiles and (b) rate constants of 4-CP degradation in the presence of PMS on $CoWO_4$ catalysts based on the synthetic pH. Experimental conditions: [$CoWO_4$] = 15 mg/30 mL, [PMS] = 1 mM, [4-CP] = 100 μM, and pH = 8.0.

Table 1
BET surface areas and pore volumes of $CoWO_4$ catalysts based on the synthetic pH conditions.

Type	Surface area (m^2/g)	Pore volume (cm^3/g)
$CoWO_4$_6	11	0.12
$CoWO_4$_7	12	0.12
$CoWO_4$_8	13	0.12
$CoWO_4$_9	25	0.22
$CoWO_4$_10	27	0.23

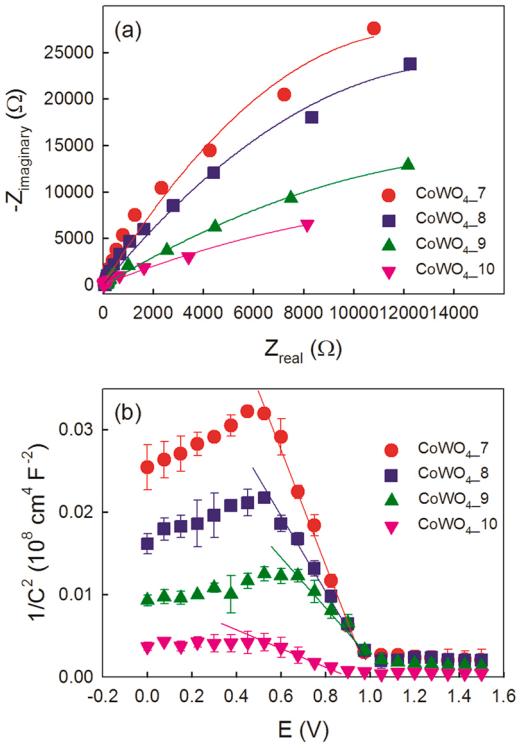

Fig. 5. (a) Nyquist and (b) Mott-Schottky plots of $CoWO_4$ catalysts based on the synthetic pH.

of PMS is the highest for $CoWO_4$_10.

3.4. Stability of $CoWO_4$ catalysts based on the synthetic pH and calcination temperature

Most metal oxide catalysts for PMS activation suffer from the leaching of metal ions from the catalysts, resulting in a decrease in catalytic activity [68,69]. Additionally, a follow-up process for the removal of leached metal ions is required if their concentrations are high. We measured the concentrations of Co and W released from $CoWO_4$ catalysts after 1 and 4 h of catalytic reactions (Fig. 6). The leaching concentrations of metal ions from $CoWO_4$_8, $CoWO_4$_9, and $CoWO_4$_10 synthesized under basic conditions were lower than those from $CoWO_4$_6 and $CoWO_4$_7 synthesized under acidic or neutral conditions (leaching concentration of Co after 1 h of catalytic reaction: $CoWO_4$_8, $CoWO_4$_9, and $CoWO_4$_10 (1.1 ~ 2.6 μM) < $CoWO_4$_6 and $CoWO_4$_7 (5.0 ~ 8.5 μM) and leaching concentration of W after 1 h of catalytic reaction: $CoWO_4$_8, $CoWO_4$_9, and $CoWO_4$_10 (4.2 ~ 9.0 μM) < $CoWO_4$_6 and $CoWO_4$_7 (20.2 ~ 20.4 μM)). Among the five $CoWO_4$

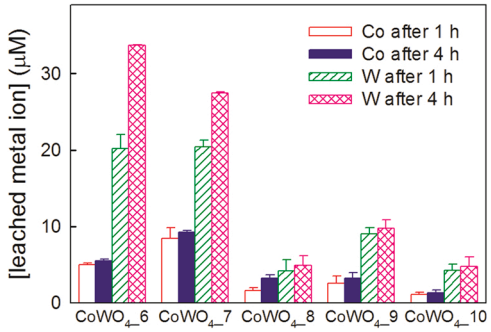

Fig. 6. Concentrations of Co and W ions leached from the $CoWO_4$ catalysts based on the synthetic pH. Experimental conditions: [$CoWO_4$] = 15 mg/30 mL, [PMS] = 1 mM, [4-CP] = 100 μM, and pH = 8.0.

catalysts tested, $CoWO_4$_10 exhibited the highest stability in terms of both Co and W leaching. Only 1.1 μM of Co and 4.2 μM of W were leached after 1 h of catalytic reaction. In addition, further catalytic reaction did not cause a significant increase in metal ion leaching (1.3 μM Co and 4.7 μM W after 4 h of catalytic reaction).

The calcination temperature in the synthesis process of $CoWO_4$ also affected its catalytic activity in PMS activation (i.e., 4-CP degradation efficiency) and stability (i.e., Co ion leaching). The catalytic activity decreased slightly, whereas the stability increased significantly with increasing calcination temperature (Fig. S6). Thus, the $CoWO_4$ catalysts synthesized at higher temperatures are considered more practical.

We compared the leaching concentration of Co in the $CoWO_4$/PMS system with those in other Co-based metal oxide/PMS systems reported in the literature. However, this should be considered only as a rough comparison because the experimental conditions such as PMS concentration, catalyst dose, solution pH, and reaction time are different for each study. As a result, $CoWO_4$ catalysts synthesized at pH 10 showed lower Co ion leaching (1.3 μM after 240 min) than most of the Co-based metal oxide catalysts previously reported (0.3 μM after 10 min ~ 381.4 μM after 15 min) (Table S5). In terms of the leaching concentration of Co/catalyst mass, the $CoWO_4$ synthesized in this study showed the highest stability (2.6 μM/g after 240 min vs. 5.7 μM/g after 120 min ~ 3814.0 μM/g after 15 min).

3.5. Degradation mechanism of organic compounds in the $CoWO_4$/PMS system

The activation of PMS by Co-based catalysts produces $SO_4^{\bullet-}$, $^{\bullet}OH$, and singlet oxygen ($^1O_2$) as oxidants, as shown in Eqs. (1)–(6). In these processes, Co^{2+} on the surface of the catalysts ($\equiv Co^{2+}$) acts as a reductant for PMS activation and is regenerated by the reaction between surface Co^{3+} ($\equiv Co^{3+}$) and PMS [70–72].

$$\equiv Co^{2+}(s) + H_2O(l) \rightarrow \equiv CoOH^{+}(s) + H^{+}(aq) \quad (1)$$

$$\equiv CoOH^{+}(s) + HSO_5^{-}(aq) \rightarrow \equiv CoO^{+}(s) + SO_4^{\bullet-}(aq) + H_2O(l) \quad (2)$$

$$SO_4^{\bullet-}(aq) + H_2O(l) \rightarrow SO_4^{2-}(aq) + {}^{\bullet}OH(aq) + H^{+}(aq) \quad (3)$$

$$\equiv CoO^{+}(s) + 2H^{+}(aq) \rightarrow \equiv Co^{3+}(s) + H_2O(l) \quad (4)$$

$$\equiv Co^{3+}(s) + HSO_5^{-}(aq) \rightarrow \equiv Co^{2+}(s) + SO_5^{\bullet-}(aq) + H^{+}(aq) \quad (5)$$

$$2SO_5^{\bullet-}(aq) + H_2O(l) \rightarrow 2HSO_4^{-}(aq) + 1.5\,{}^1O_2(g) \quad (6)$$

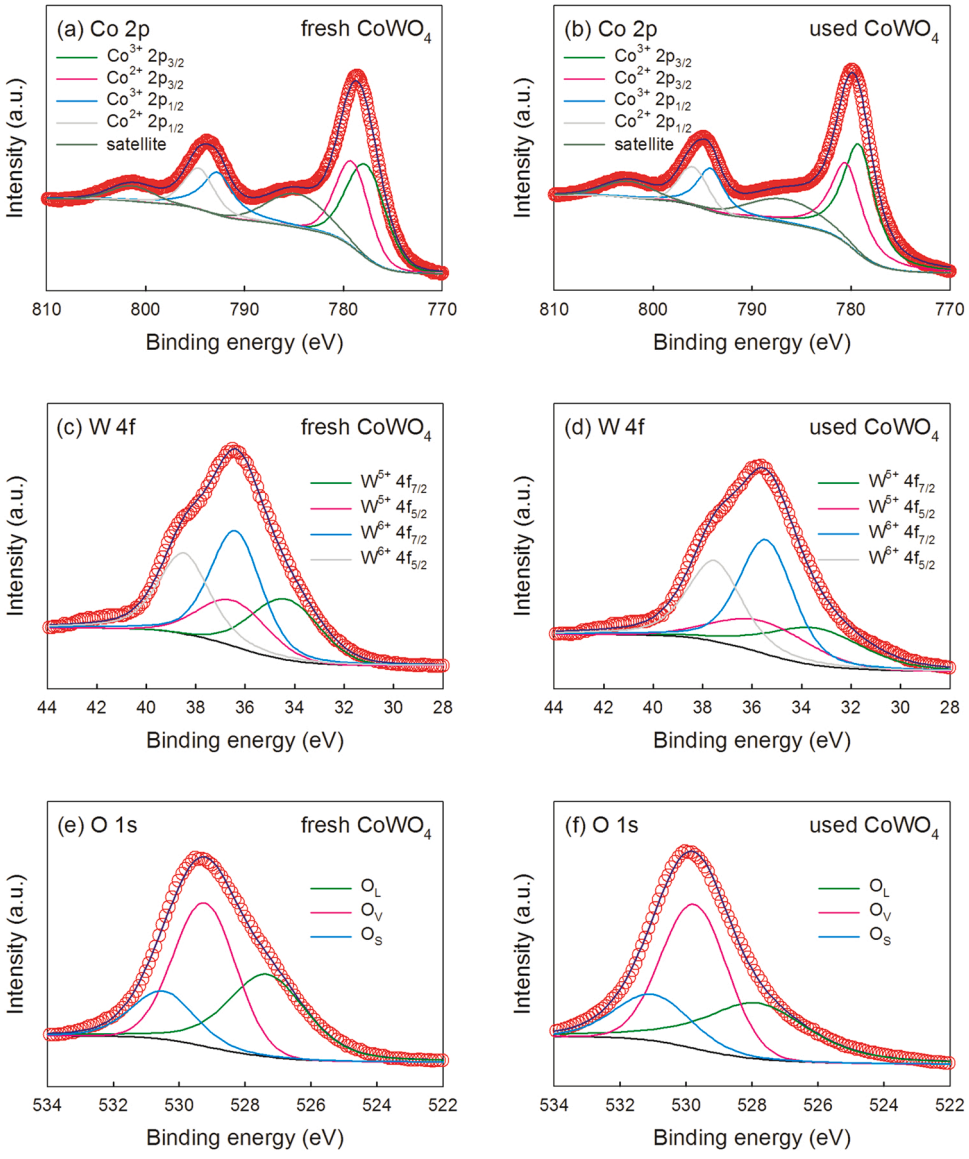

Fig. 7. XPS spectra of (a and b) Co 2p, (c and d) W 4f, and (e and f) O 1s for fresh and used $CoWO_4$ catalysts.

The elemental chemical states of the fresh and used $CoWO_4$ samples (before and after the catalytic reaction for 4-CP degradation in the presence of PMS (5 min)) were analyzed by XPS (Fig. 7). The Co 2p XPS spectra of the fresh and used $CoWO_4$ catalysts are shown in Fig. 7a and b, respectively. The peaks at 779.1 and 794.6 eV with spin-orbit splitting (ΔE) of 15.5 eV are assigned to Co^{2+} $2p_{3/2}$ and $2p_{1/2}$, respectively. The peaks at 777.7 and 792.7 eV with ΔE of 15.0 eV correspond to Co^{3+} $2p_{3/2}$ and $2p_{1/2}$, respectively [27,73]. Two shakeup satellite peaks are also observed at 784.7 and 801.5 eV in the Co 2p XPS spectra [32,74]. The relative ratio of Co^{2+}/Co^{3+} on $CoWO_4$ slightly decreased from 0.80 to 0.76 after the catalytic reaction. This result indicates that Co^{2+} ions on the surface of $CoWO_4$ are involved in the reductive activation of PMS [75,76].

Similar behavior was observed in the W 4f XPS spectra (Fig. 7c and d). Two doublet peaks (one appears at 34.4 eV for W $4f_{7/2}$ and 36.5 eV for W $4f_{5/2}$; the other appears at 36.4 eV for W $4f_{7/2}$ and 38.5 eV for W $4f_{5/2}$) can be attributed to W^{5+} and W^{6+} [77,78]. The relative ratio of W^{5+}/W^{6+} (0.60) for fresh $CoWO_4$ was slightly higher than that (0.56) for used $CoWO_4$. This result implies that the W^{5+} on the $CoWO_4$ surface ($\equiv W^{5+}$) can also activate PMS to produce $SO_4^{\bullet-}$ like Co^{2+} on the $CoWO_4$ surface (Eqs. (1) and (2)).

The O 1s XPS spectra of $CoWO_4$ catalysts contain three peaks at 527.3, 529.2, and 530.5 eV, which correspond to the lattice oxygen species (O_L, O^{2-}), oxygen vacancy (O_V, O_2^{2-}/O^-), and surface adsorbed oxygen (O_S, $H_2O/O_2/-OH$), respectively (Fig. 7e and f) [79,80]. The percentages of O_L, O_V, and O_S on fresh $CoWO_4$ were 38.1%, 44.8%, and 17.1%, respectively. These values on used $CoWO_4$ were 35.4%, 46.1%, and 18.5%, respectively. The decrease in O_L after the catalytic reaction could be attributed to the O_L-induced reduction of Co^{3+} to Co^{2+} (also reduction of W^{6+} to W^{5+}) [81,82]. This regeneration of Co^{2+} by O_L can help maintain a constant catalytic activity for PMS activation.

To identify the main oxidant involved in the degradation of 4-CP in the $CoWO_4$/PMS system, quenching experiments were performed using *tert*-butyl alcohol or methanol as radical scavengers (Fig. 8a). Methanol can effectively scavenge both $^{\bullet}OH$ and $SO_4^{\bullet-}$; however, *tert*-butyl alcohol selectively reacts with $^{\bullet}OH$ (k for methanol + $^{\bullet}OH$ = 9.7×10^8, k for methanol + $SO_4^{\bullet-}$ = 2.5×10^7, k for *tert*-butyl alcohol + $^{\bullet}OH$ = 6.0×10^8, and k for *tert*-butyl alcohol + $SO_4^{\bullet-}$ = 4.0×10^5 M^{-1} s^{-1}) [83,84]. Methanol significantly inhibited the degradation of 4-CP. The increase in the methanol concentration from 0.1 M to 1.0 M further reduced the degradation efficiency of 4-CP after 5 min from 60.8% to 47.1%. However, *tert*-butyl alcohol (1.0 M) had little effect on the kinetics of 4-CP degradation. This result suggests that the degradation of 4-CP primarily occurs via the reaction of $SO_4^{\bullet-}$ with 4-CP.

To provide convincing evidence for the involvement of $SO_4^{\bullet-}$ in the degradation process, the radical species produced in the $CoWO_4$/PMS system were identified via ESR analysis using BMPO as a spin-trapping agent (Fig. 8b). ESR signals corresponding to BMPO-$SO_4^{\bullet-}$ were clearly observed; however, characteristic peaks of BMPO-$^{\bullet}OH$ were absent. This agrees well with the results of quenching experiments, which show that $SO_4^{\bullet-}$ is the main oxidant in the $CoWO_4$/PMS system.

Notably, excess methanol (1.0 M) did not completely prevent 4-CP degradation. This result suggests that another oxidant (or mechanism) contributed to the degradation of 4-CP in the $CoWO_4$/PMS system. $^1O_2$ can be produced in Co-based catalyst/PMS systems via the hydrolysis of $SO_5^{\bullet-}$ (Eq. (6)) and the reaction between O_V and PMS ($O_V(s) \rightarrow O^*(s)$ (active oxygen); $O^*(s) + HSO_5^-(aq) \rightarrow HSO_4^-(aq) + {}^1O_2(g)$) [85,86]. We compared the degradation kinetics of 4-CP in deionized water (H_2O) with those in deuterium oxide (D_2O) to investigate whether $^1O_2$ was involved in the degradation process (Fig. 8c). The lifetime of $^1O_2$ in D_2O is approximately ten times longer than that in H_2O [87]. Therefore, the degradation of 4-CP should be enhanced when D_2O is used as a solvent as far as $^1O_2$ is concerned. However, the degradation rate of 4-CP in D_2O was similar to that in H_2O. This result can rule out the possibility of 4-CP degradation by $^1O_2$ in the $CoWO_4$/PMS system. In addition, the effect of dissolved oxygen (i.e., N_2 gas purging) on the degradation of 4-CP in the $CoWO_4$/PMS system was negligible (Fig. S7).

The PMS activation can also proceed through a nonradical mechanism when heterogeneous metal oxides are used as catalysts. Metal oxides can facilitate electron transfer from organic compounds to PMS by forming PMS-metal oxide complexes ($\equiv M^{x+}-OH(s) + HSO_5^-(aq) \rightarrow \equiv M^{x+}-OSO_4^-(s) + H_2O(l)$) and enhance the degradation of organic compounds without producing radical species [88–90]. The changes in the PMS concentration in the presence of 4-CP alone, $CoWO_4$ alone, and both 4-CP and $CoWO_4$ were monitored (Fig. 8d). PMS did not decompose in the presence of 4-CP alone. The PMS concentration gradually

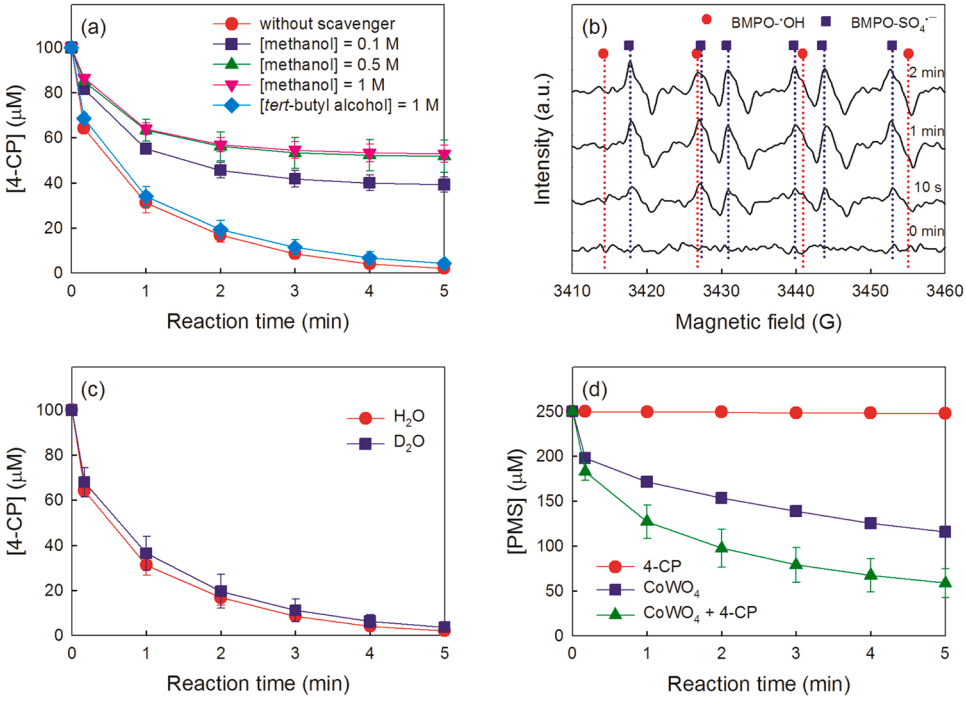

Fig. 8. (a) Effects of radical scavengers on the degradation kinetics of 4-CP in the $CoWO_4$/PMS system. (b) ESR spectra recorded in the $CoWO_4$/PMS system. (c) Degradation of 4-CP by the $CoWO_4$/PMS system in H_2O and D_2O. (d) Decomposition of PMS by 4-CP alone, $CoWO_4$ alone, and both $CoWO_4$ and 4-CP. Experimental conditions: [$CoWO_4$] = 15 mg/30 mL, [PMS] = 0.25 mM for parts (a), (c), and (d) or 1 mM for part (b), [4-CP] = 100 μM for parts (a), (c), and (d), [methanol] or [*tert*-butyl alcohol] = 0.1, 0.5, or 1 M for part (a), [BMPO] = 1 mM for part (b), and pH = 8.0.

decreased with reaction time in the presence of $CoWO_4$ because of the reduction of PMS to radical species (Eqs. (1) and (2)). The PMS decomposition rate was more significant in the presence of both 4-CP and $CoWO_4$ than in the presence of $CoWO_4$ alone. This result indirectly implies that electron transfer from 4-CP to PMS is effectively facilitated by $CoWO_4$.

Chronoamperometry experiments were performed to clearly show the nonradical reaction pathway (i.e., electron transfer from 4-CP to the PMS-$CoWO_4$ complexes) (Fig. 9). The injection of PMS generated a negative current owing to electron transfer from the $CoWO_4$ electrode to the PMS. When 4-CP was injected, positive current flow was observed. This phenomenon confirms that electron transfer from the 4-CP to the $CoWO_4$ electrode is possible in the presence of PMS.

3.6. Effects of reaction parameters on organic compound degradation in the $CoWO_4$/PMS system

The degradation kinetics of 4-CP in the $CoWO_4$/PMS system was investigated as a function of the PMS concentration and $CoWO_4$ dosage. The results are expressed in terms of first-order rate constants for 4-CP degradation (k). The k value increased with increasing PMS concentration, up to 2 mM (Fig. 10a). There was also a positive correlation between the k value and $CoWO_4$ dosage up to 1 g/L (Fig. 10b). Increasing the PMS concentration or $CoWO_4$ dosage increases the interaction between PMS and $CoWO_4$ for the production of $SO_4^{\bullet-}$ and the formation of PMS-$CoWO_4$ complexes, which accelerates the degradation of 4-CP through radical and nonradical mechanisms.

Fig. 10c shows the degradation kinetics of 4-CP in the $CoWO_4$/PMS system under different initial concentrations of 4-CP. The results are expressed in terms of C/C_0, where C and C_0 are the concentrations of 4-CP at reaction times t and 0 min, respectively. The degradation efficiency decreased with increasing initial 4-CP concentration. This is because, at higher concentrations of 4-CP, greater amounts of $SO_4^{\bullet-}$ and PMS-$CoWO_4$ complexes are required to degrade the same percentage of 4-CP. 4-CP was completely degraded within 10 s at [4-CP] = 50 μM, 1 min at [4-CP] = 100 μM, 3 min at [4-CP] = 250 μM, and 7.5 min at [4-CP] = 500 μM. However, the final degradation efficiency was 77.3% (not 100%) at [4-CP] = 1 mM owing to the depletion of PMS.

We also examined the effects of background anions and humic acid on the degradation kinetics of 4-CP in the $CoWO_4$/PMS system (Fig. 10d). All background anions (chloride (Cl^-), nitrate (NO_3^-), bicarbonate (HCO_3^-), and hydrogen phosphate (HPO_4^{2-})) reduced the degradation of 4-CP because they can inhibit the $SO_4^{\bullet-}$-mediated degradation of 4-CP by scavenging $SO_4^{\bullet-}$ [91,92]. However, 4-CP was completely degraded within 1 min, even in the presence of a high concentration of anions (10 mM). Because humic acid can also act as $SO_4^{\bullet-}$ scavenger [93,94], the degradation of 4-CP was reduced in the presence of humic acid (10 ppm) with the concurrent degradation of humic acid

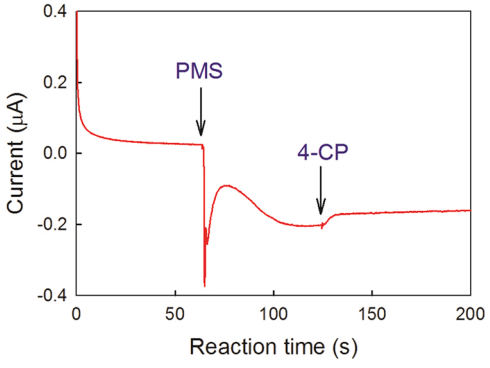

Fig. 9. Current responses upon the injection of PMS and 4-CP. Experimental conditions: injected [PMS] = 1 mM, injected [4-CP] = 100 μM, [$NaClO_4$] = 50 mM, pH = 8.0, and bias potential = 0.0 V vs. Ag/AgCl electrode.

(Fig. S8). However, the inhibitory effect of humic acid was also insignificant. A significant decrease in degradation efficiency in the presence of background anions and humic acid is often found in the radical mechanism-based PMS activation processes [95,96]. Because the degradation occurs through not only a radical mechanism but also a nonradical mechanism in the $CoWO_4$/PMS system, their inhibitory effects are limited.

3.7. Practical applications of the $CoWO_4$/PMS system for water treatment

The applicability of water treatment systems to diverse organic compounds is an important requirement from a practical point of view. Therefore, the degradation kinetics of organic compounds in the $CoWO_4$/PMS system were measured for 16 organic compounds: phenol, 2-chlorophenol, 2-nitrophenol, 4-CP, 4-nitrophenol, 4-bromophenol, 4-methylphenol, 2,4-dimethylphenol, 2,4-dichlorophenol, bisphenol A, propranolol, sulfisoxazole, sulfamethoxazole, sulfanilamide, cimetidine, and ranitidine (Table 2 and Fig. S9). The k values varied according to the type of organic compound used. This behavior is because the reactivity of $SO_4^{\bullet-}$ and the PMS-$CoWO_4$ complexes toward organic compounds differs depending on their type. Despite the difference in the k values, all the tested organic compounds were rapidly degraded in the $CoWO_4$/PMS system. Complete degradation was achieved within 4 min, except for 4-nitrophenol. This feature allows for the use of $CoWO_4$ as a PMS activator for the treatment of multicomponent wastewater.

When the k values of phenol and substituted phenols were plotted against the Hammett constants (σ^+), which represent the relative electron densities in aromatic rings [97], the chemical properties of the organic compounds that were efficiently degraded in the $CoWO_4$/PMS system were determined (Fig. 11). The k increased with decreasing σ^+ in the case of substituted phenols with $\sigma^+ > 0$ (electron-withdrawing groups). This result implies that electron-rich organic compounds are more rapidly degraded in the $CoWO_4$/PMS system. However, the k slightly decreased with decreasing σ^+ for substituted phenols with $\sigma^+ < 0$ (electron-donating groups). Although the electron density increases with decreasing σ^+, the steric bulk of the methyl group hinders the adsorption of organic compounds on the surface of $CoWO_4$ and/or the approach of $SO_4^{\bullet-}$ to the aromatic ring. This behavior can reduce the degradation of organic compounds by inhibiting mediated electron transfer (nonradical mechanism) and $SO_4^{\bullet-}$ attack (radical mechanism).

Multiple degradation experiments were performed to verify the reusability of the $CoWO_4$ catalysts. The degradation of 4-CP was repeated for ten cycles (Fig. 12). Aliquots of 4-CP (100 μM) and PMS (1 mM) were added to the reactor after each degradation cycle; however, the initial $CoWO_4$ catalysts were reused without surface cleaning. A 100% degradation was achieved over ten repeated cycles. This result demonstrates that the $CoWO_4$ synthesized in this study exhibits high resistance against catalyst deactivation.

We compared the catalytic activity of synthesized $CoWO_4$ for the degradation of 4-CP in the presence of PMS with those of other Co-based metal oxides such as synthesized Co_3O_4, commercial CoO, Co_3O_4, $CoWO_4$, $CoFe_2O_4$, $CoAl_2O_4$, and $LiCoO_2$. All the tested Co-based metal oxides exhibited catalytic activity for 4-CP degradation through PMS activation. However, the degradation rate largely depended on the type of catalyst used. Complete degradation of 4-CP was achieved within 1 min on $CoWO_4$ synthesized in this study, whereas it took more than 3 min on other Co-based metal oxides (Fig. 13a). In terms of the k value, the degradation performance of $CoWO_4$ synthesized in this study was 2.4−83.6 times better than those of other Co-based metal oxides (Fig. 13b).

To assess the impact of practical conditions on the degradation activity of the $CoWO_4$/PMS system, the degradation kinetics of 4-CP in tap water was investigated and compared with that in deionized water. Solutions and suspensions prepared in tap water were used in the experiments. Although tap water contained various ions (Table S6), the

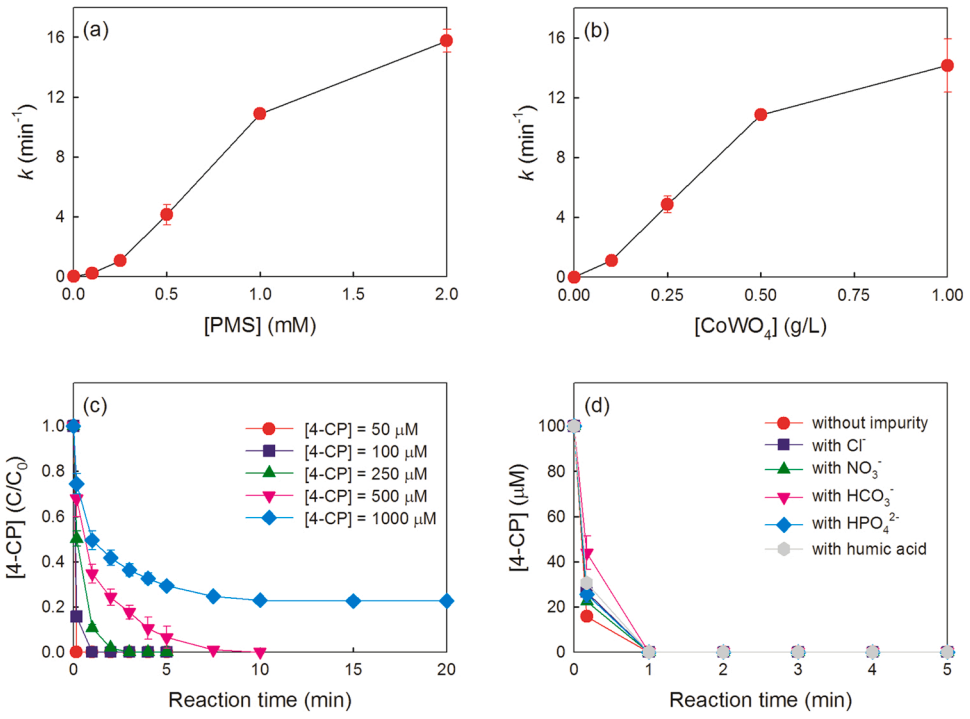

Fig. 10. Effects of the (a) PMS concentration, (b) $CoWO_4$ dosage, and (c) initial 4-CP concentration on the degradation rate of 4-CP in the $CoWO_4$/PMS system. (d) Time profile of 4-CP concentration in the $CoWO_4$/PMS system with and without background anions or humic acid. Experimental conditions: [$CoWO_4$] = 15 mg/30 mL for parts (a), (c), and (d), [PMS] = 1 mM for parts (b), (c), and (d), [4-CP] = 100 μM for parts (a), (b), and (d), [anion] = 10 mM for part (d), [humic acid] = 10 ppm for part (d), and pH = 8.0.

Table 2
First-order degradation rate constants (k) of various organic compounds in the $CoWO_4$/PMS system[a].

Type	k (min^{-1})	Type	k (min^{-1})
phenol	14.29 ± 0.08	2,4-dichlorophenol	18.51 ± 0.18
2-chlorophenol	11.86 ± 0.05	bisphenol A	11.96 ± 0.08
2-nitrophenol	2.70 ± 0.31	propranolol	1.50 ± 0.24
4-CP	10.86 ± 0.07	sulfamethoxazole	6.78 ± 0.17
4-nitrophenol	0.53 ± 0.05	sulfisoxazole	13.78 ± 0.06
4-bromophenol	10.18 ± 0.15	sulfanilamide	5.27 ± 0.15
4-methylphenol	9.95 ± 0.01	cimetidine	n.d.[b]
2,4-dimethylphenol	9.42 ± 0.11	ranitidine	n.d.

[a] Experimental conditions: [$CoWO_4$] = 15 mg/30 mL, [PMS] = 1 mM, [organic compound] = 100 μM, and pH = 8.0. [b] Not determined because of very rapid degradation.

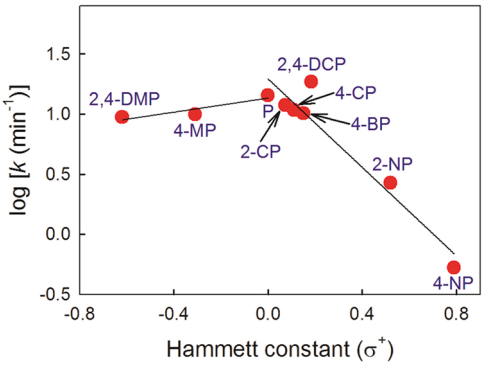

Fig. 11. Relationship between the degradation rate constants (k) and the Hammett constants (σ^+). Experimental conditions: [$CoWO_4$] = 15 mg/30 mL, [PMS] = 1 mM, [phenol] or [substituted phenol] = 100 μM, and pH = 8.0. P: phenol, 2-CP: 2-chlorophenol, 2-NP: 2-nitrophenol, 4-CP: 4-chlorophenol, 4-NP: 4-nitrophenol, 4-BP: 4-bromophenol, 4-MP: 4-methylphenol, 2,4-DMP: 2,4-dimethylphenol, and 2,4-DCP: 2,4-dichlorophenol.

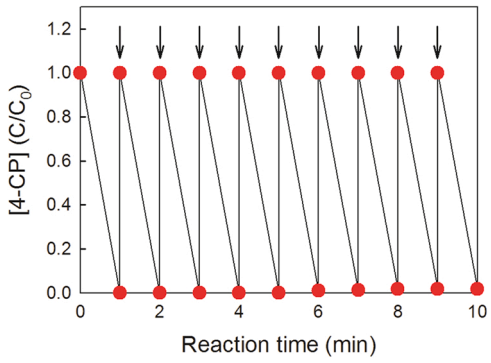

Fig. 12. Multiple cycles of 4-CP degradation in the $CoWO_4$/PMS system. Experimental conditions: [$CoWO_4$] = 15 mg/30 mL, [PMS] = 1 mM, [4-CP] = 100 μM, and pH = 8.0. 4-CP (100 μM) and PMS (1 mM) were repeatedly added to the reactor at the beginning of each cycle (i.e., at the time indicated by arrows).

degradation rate of 4-CP in tap water was similar to that in deionized water (Fig. S10).

4. Conclusions

Among various PMS activation methods for the degradation of aqueous organic compounds, a heterogeneous catalytic system has been considered more practical than energy- and chemical-induced methods [98,99] because a heterogeneous catalytic system does not require a large amount of energy or the continuous addition of a chemical activator. In this study, we synthesized $CoWO_4$ nanoparticles under various pH conditions using a hydrothermal method and used them as PMS activators for water treatment. The physical and chemical properties were significantly affected by the synthetic pH. The $CoWO_4$ prepared at pH 10 exhibited the highest catalytic activity for PMS activation (i.e., organic compound degradation) and stability for metal ion leaching. 4-CP at 100 μM concentration was completely degraded within 1 min in the presence of 15 mg of $CoWO_4$_10 and 1 mM PMS when the total

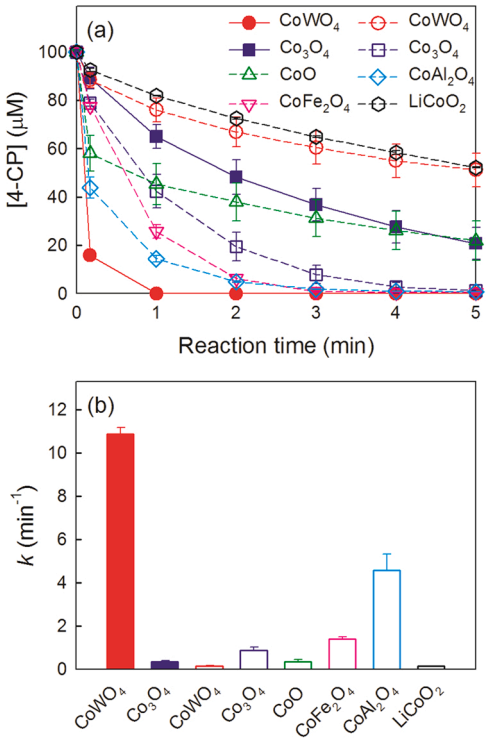

Fig. 13. (a) Time profiles and (b) rate constants of 4-CP degradation in the various Co-based metal oxide/PMS systems. Experimental conditions: [catalyst] = 15 mg/30 mL, [PMS] = 1 mM, [4-CP] = 100 μM, and pH = 8.0. Filled symbols (or solid bars) represent materials synthesized in this study and empty symbols (or open bars) represent commercial materials.

volume of the solution was 30 mL. Only 1.3 μM Co and 4.7 μM W were leached from $CoWO_4$_10 after 4 h of the catalytic reaction. The effects of anions and humic acid, which are commonly present in water and wastewater, were insignificant in the $CoWO_4$/PMS system. The $CoWO_4$ synthesized in this study exhibited superior activity compared to other Co-based metal oxides (k for 4-CP degradation of $CoWO_4$_10 = 10.87 min^{-1} vs. k for 4-CP degradation of other Co-based metal oxides = 0.13 ~ 4.56 min^{-1}). Various organic compounds were rapidly degraded in the $CoWO_4$/PMS system (k = 0.53 (4-nitrophenol) ~ 18.51 min^{-1} (2, 4-dichlorophenol)). In addition, the PMS activation ability of $CoWO_4$ was not reduced by repeated use. Based on the aforementioned advantages, $CoWO_4$, especially that synthesized at pH 10, can be proposed as a practical PMS activator for the degradation of organic compounds in water.

CRediT authorship contribution statement

Anh Quoc Khuong Nguyen: Conceptualization, Investigation, Visualization, Writing – original draft, Writing – review & editing. **Yong-Yoon Ahn:** Investigation, Formal analysis, Writing – review & editing. **Gwanyong Shin:** Investigation, Writing – review & editing. **Younsang Cho:** Formal analysis, Writing – review & editing. **Jonghun Lim:** Writing – review & editing. **Kitae Kim:** Writing – review & editing. **Jungwon Kim:** Conceptualization, Writing – original draft, Writing – review & editing, Project administration, Funding acquisition, Supervision.

Declaration of Competing Interest

The authors declare that they have no known competing financial interests or personal relationships that could have appeared to influence the work reported in this paper.

Data Availability

Data will be made available on request.

Acknowledgements

This work was supported by the National Research Foundation of Korea (NRF) grant funded by the Korea government (Ministry of Science and ICT) (NRF-2022R1A2C1003215).

Appendix A. Supporting information

Supplementary data associated with this article can be found in the online version at doi:10.1016/j.apcatb.2022.122266.

References

[1] F. Ghanbari, M. Moradi, Application of peroxymonosulfate and its activation methods for degradation of environmental organic pollutants: review, Chem. Eng. J. 310 (2017) 41–62.
[2] S. Xiao, M. Cheng, H. Zhong, Z. Liu, Y. Liu, X. Yang, Q. Liang, Iron-mediated activation of persulfate and peroxymonosulfate in both homogeneous and heterogeneous ways: a review, Chem. Eng. J. 384 (2020), 123265.
[3] X. Yang, X. Ding, L. Zhou, Q. Zhao, Y. Ji, X. Wang, J.-M. Chovelon, G. Xiu, Direct oxidation of antibiotic trimethoprim by unactivated peroxymonosulfate via a nonradical transformation mechanism, Chemosphere 263 (2021), 128194.
[4] Y. Zhou, Y. Gao, J. Jiang, Y.-M. Shen, S.-Y. Pang, Z. Wang, J. Duan, Q. Guo, C. Guan, J. Ma, Transformation of tetracycline antibiotics during water treatment with unactivated peroxymonosulfate, Chem. Eng. J. 379 (2020), 122378.
[5] X. Liao, J. Cao, Y. Hu, C. Zhang, L. Hu, Mechanism of unactivated peroxymonosulfate-induced degradation of methyl parathion: kinetics and transformation pathway, Chemosphere 284 (2021), 131332.
[6] Y. Zhang, B. Wang, X. Hu, H. Li, Non-activated peroxymonosulfate oxidation of *p*-aminobenzoic acid in the presence of effluent organic matter, Chem. Eng. J. 384 (2020), 123247.
[7] J. Wang, S. Wang, Activation of persulfate (PS) and peroxymonosulfate (PMS) and application for the degradation of emerging contaminants, Chem. Eng. J. 334 (2018) 1502–1517.
[8] R. Yin, W. Guo, H. Wang, J. Du, X. Zhou, Q. Wu, H. Zheng, J. Chang, N. Ren, Selective degradation of sulfonamide antibiotics by peroxymonosulfate alone: direct oxidation and nonradical mechanisms, Chem. Eng. J. 334 (2018) 2539–2546.
[9] H. Milh, D. Cabooter, R. Dewil, Role of process parameters in the degradation of sulfamethoxazole by heat-activated peroxymonosulfate oxidation: radical identification and elucidation of the degradation mechanism, Chem. Eng. J. 422 (2021), 130457.
[10] Y. Lee, S. Lee, M. Cui, Y. Ren, B. Park, J. Ma, Z. Han, J. Khim, Activation of peroxodisulfate and peroxymonosulfate by ultrasound with different frequencies: impact on ibuprofen removal efficient, cost estimation and energy analysis, Chem. Eng. J. 413 (2021), 127487.
[11] Y. Hu, T. Zhang, L. Jiang, S. Yao, H. Ye, K. Lin, C. Cui, Removal of sulfonamide antibiotic resistant bacterial and intracellular antibiotic resistance genes by UVC-activated peroxymonosulfate, Chem. Eng. J. 368 (2019) 888–895.
[12] Y. Feng, D. Wu, Y. Zhou, K. Shih, A metal-free method of generating sulfate radicals through direct interaction of hydroxylamine and peroxymonosulfate: mechanisms, kinetics, and implications, Chem. Eng. J. 330 (2017) 906–913.
[13] S. Zhou, Y. Yu, W. Zhang, X. Meng, J. Luo, L. Deng, Z. Shi, J. Crittenden, Oxidation of microcystin-LR via activation of peroxymonosulfate using ascorbic acid: kinetic modeling and toxicity assessment, Environ. Sci. Technol. 52 (2018) 4305–4312.
[14] N.S. Shah, J.A. Khan, M. Sayed, Z.U.H. Khan, J. Iqbal, M. Imran, B. Murtaza, A. Zakir, K. Polychronopoulou, Nano zerovalent zinc catalyzed peroxymonosulfate based advanced oxidation technologies for treatment of chlorpyrifos in aqueous solution: a semi-pilot scale study, J. Clean. Prod. 246 (2020), 119032.
[15] H. Lee, H.-i. Kim, S. Weon, W. Choi, Y.S. Hwang, J. Seo, C. Lee, J.-H. Kim, Activation of persulfates by graphitized nanodiamonds for removal of organic compounds, Environ. Sci. Technol. 50 (2016) 10134–10142.
[16] E.-T. Yun, J.H. Lee, J. Kim, H.-D. Park, J. Lee, Identifying the nonradical mechanism in the peroxymonosulfate activation process: singlet oxygenation versus mediated electron transfer, Environ. Sci. Technol. 52 (2018) 7032–7042.
[17] Y.-Y. Ahn, H. Bae, H.-I. Kim, S.-H. Kim, J.-H. Kim, S.-G. Lee, J. Lee, Surface-loaded metal nanoparticles for peroxymonosulfate activation: efficiency and mechanism reconnaissance, Appl. Catal. B Environ. 241 (2019) 561–569.
[18] L. Wang, H. Xu, N. Jiang, Z. Wang, J. Jiang, T. Zhang, Trace cupric species triggered decomposition of peroxymonosulfate and degradation of organic pollutants: Cu(III) being the primary and selective intermediate oxidant, Environ. Sci. Technol. 54 (2020) 4686–4694.
[19] X. Lai, X.-a. Ning, J. Chen, Y. Li, Y. Zhang, Y. Yuan, Comparison of the Fe^{2+}/H_2O_2 and Fe^{2+}/PMS systems in simulated sludge: removal of PAHs, migration of elements and formation of chlorination by-products, J. Hazard. Mater. 398 (2020), 122826.

[20] M. Chen, L. Zhu, S. Liu, R. Li, N. Wang, H. Tang, Efficient degradation of organic pollutants by low-level Co^{2+} catalyzed homogeneous activation of peroxymonosulfate, J. Hazard. Mater. 371 (2019) 456–462.

[21] G.P. Anipsitakis, D.D. Dionysiou, Radical generation by the interaction of transition metals with common oxidants, Environ. Sci. Technol. 38 (2004) 3705–3712.

[22] B. Bouzayani, E. Rosales, M. Pazos, S.C. Elaoud, M.A. Sanromán, Homogeneous and heterogeneous peroxymonosulfate activation by transition metals for the degradation of industrial leather dye, J. Clean. Prod. 228 (2019) 222–230.

[23] G.P. Anipsitakis, E. Stathatos, D.D. Dionysiou, Heterogeneous activation of Oxone using Co_3O_4, J. Phys. Chem. B 109 (2005) 13052–13055.

[24] J. Hou, X. He, S. Zhang, J. Yu, M. Feng, X. Li, Recent advances in cobalt-activated sulfate radical-based advanced oxidation processes for water remediation: a review, Sci. Total Environ. 770 (2021), 145311.

[25] P. Hu, M. Long, Cobalt-catalyzed sulfate radical-based advanced oxidation: a review on heterogeneous catalysts and applications, Appl. Catal. B Environ. 181 (2016) 103–117.

[26] Q. Yang, H. Choi, S.R. Al-Abed, D.D. Dionysiou, Iron–cobalt mixed oxide nanocatalysts: heterogeneous peroxymonosulfate activation, cobalt leaching, and ferromagnetic properties for environmental applications, Appl. Catal. B Environ. 88 (2009) 462–469.

[27] X. Zhang, Z. Yang, X. Cui, W. Liu, B. Zou, W. Liao, Cobalt/calcium bimetallic oxides based on bio-waste eggshells for the efficient degradation of norfloxacin by peroxymonosulfate activation, J. Colloid Interface Sci. 621 (2022) 1–11.

[28] C. Yin, Q. Xia, J. Zhou, B. Li, Y. Guo, A. Khan, X. Li, A. Xu, Direct electron transfer process-based peroxymonosulfate activation via surface labile oxygen over mullite oxide YMn_2O_5 for effective removal of bisphenol A, Sep. Purif. Technol. 280 (2022), 119924.

[29] H. Li, H. Wang, Q. Gao, B. Han, K. Xia, C. Zhou, Hierarchical flower-like Co_2TiO_4 nanosheets with unique structural and compositional advantages to boost peroxymonosulfate activation for degradation of organic pollutants, J. Mater. Chem. A 8 (2020) 20953–20962.

[30] Y. Wang, S. Zhao, W. Fan, Y. Tian, X. Zhao, The synthesis of novel Co-Al_2O_3 nanofibrous membranes with efficient activation of peroxymonosulfate for bisphenol A degradation, Environ. Sci. Nano 5 (2018) 1933–1942.

[31] Y. Yao, Y. Cai, G. Wu, F. Wei, X. Li, H. Chen, S. Wang, Sulfate radicals induced from peroxymonosulfate by cobalt manganese oxides ($Co_xMn_{3-x}O_4$) for Fenton-Like reaction in water, J. Hazard. Mater. 296 (2015) 128–137.

[32] P. Cai, J. Zhao, X. Zhang, T. Zhang, G. Yin, S. Chen, C.-L. Dong, Y.-C. Huang, Y. Sun, D. Yang, B. Xing, Synergy between cobalt and nickel on $NiCo_2O_4$ nanosheets promotes peroxymonosulfate activation for efficient norfloxacin degradation, Appl. Catal. B Environ. 306 (2022), 121091.

[33] L. Liu, H. Mi, M. Zhang, F. Sun, R. Zhan, H. Zhao, S. He, L. Zhou, Efficient moxifloxacin degradation by $CoFe_2O_4$ magnetic nanoparticles activated peroxymonosulfate: kinetics, pathways and mechanisms, Chem. Eng. J. 407 (2021), 127201.

[34] C.-X. Li, C.-B. Chen, J.-Y. Lu, S. Cui, J. Li, H.-Q. Liu, W.-W. Li, F. Zhang, Metal organic framework-derived $CoMn_2O_4$ catalyst for heterogeneous activation of peroxymonosulfate and sulfanilamide degradation, Chem. Eng. J. 337 (2018) 101–109.

[35] C. Chen, L. Liu, Y. Li, W. Li, L. Zhou, Y. Lan, Y. Li, Insight into heterogeneous catalytic degradation of sulfamethazine by peroxymonosulfate activated with $CuCo_2O_4$ derived from bimetallic oxalate, Chem. Eng. J. 384 (2020), 123257.

[36] X. Tian, C. Tian, Y. Nie, C. Dai, C. Yang, N. Tian, Z. Zhou, Y. Li, Y. Wang, Controlled synthesis of dandelion-like $NiCo_2O_4$ microspheres and their catalytic performance for peroxymonosulfate activation in humic acid degradation, Chem. Eng. J. 331 (2018) 144–151.

[37] S.B. Hammouda, F. Zhao, Z. Safaei, V. Srivastava, D.L. Ramasamy, S. Iftekhar, S. Kalliola, M. Sillanpää, Degradation and mineralization of phenol in aqueous medium by heterogeneous monopersulfate activation on nanostructured cobalt based-perovskite catalysts $ACoO_3$ (A = La, Ba, Sr and Ce): characterization, kinetics and mechanism study, Appl. Catal. B Environ. 215 (2017) 60–73.

[38] M. Sivakumar, R. Madhu, S.-M. Chen, V. Veeramani, A. Manikandan, W.H. Hung, N. Miyamoto, Y.-L. Chueh, Low-temperature chemical synthesis of $CoWO_4$ nanospheres for sensitive nonenzymatic glucose sensor, J. Phys. Chem. C 120 (2016) 17024–17028.

[39] X. Xing, Y. Gui, G. Zhang, C. Song, $CoWO_4$ nanoparticles prepared by two methods displaying different structures and supercapacitive performances, Electrochim. Acta 157 (2015) 15–22.

[40] C. Ling, L.Q. Zhou, H. Jia, First-principles study of crystalline $CoWO_4$ as oxygen evolution reaction catalyst, RSC Adv. 4 (2014) 24692–24697.

[41] A. Tiwari, V. Singh, T.C. Nagaiah, Non-noble cobalt tungstate catalyst for effective electrocatalytic oxidation of borohydride, ACS Appl. Mater. Interfaces 11 (2019) 21465–21472.

[42] P.K. Pandey, N.S. Bhave, R.B. Kharat, Characterization of spray deposited $CoWO_4$ thin films for photovoltaic electrochemical studies, J. Mater. Sci. 42 (2007) 7927–7933.

[43] J. Wang, L. Yang, L. Zhang, Constructed 3D hierarchical micro-flowers $CoWO_4$@ Bi_2WO_6 Z-scheme heterojunction catalyzer: two-channel photocatalytic H_2O_2 production and antibiotics degradation, Chem. Eng. J. 420 (2021), 127639.

[44] X. Liu, J. Shu, H. Wang, Z. Jiang, L. Xu, C. Liu, One-pot preparation of a novel $CoWO_4/ZnWO_4$ p-n heterojunction photocatalyst for enhanced photocatalytic activity under visible light irradiation, J. Phys. Chem. Solids 172 (2023), 111061.

[45] H. Cui, B. Li, Y. Zhang, X. Zheng, X. Li, Z. Li, S. Xu, Constructing Z-scheme based $CoWO_4$/CdS photocatalysts with enhanced dye degradation and H_2 generation performance, Int. J. Hydrog. Energy 43 (2018) 18242–18252.

[46] S.L. Prabavathi, K. Govindan, K. Saravanakumar, A. Jang, V. Muthuraj, Construction of heterostructure $CoWO_4$/g-C_3N_4 nanocomposite as an efficient visible-light photocatalyst for norfloxacin degradation, J. Ind. Eng. Chem. 80 (2019) 558–567.

[47] J. Qiao, H. Zhang, G. Li, S. Li, Z. Qu, M. Zhang, J. Wang, Y. Song, Fabrication of a novel Z-scheme $SrTiO_3/Ag_2S/CoWO_4$ composite and its application in sonocatalytic degradation of tetracyclines, Sep. Purif. Technol. 211 (2019) 843–856.

[48] L. Xu, N.-P. Liu, H.-L. An, W.-T. Ju, B. Liu, X.-F. Wang, X. Wang, Preparation of $Ag_3PO_4/CoWO_4$ S-scheme heterojunction and study on sonocatalytic degradation of tetracycline, Ultrason. Sonochem. 89 (2022), 106147.

[49] A. Mills, N. Elliott, G. Hill, D. Fallis, J.R. Durrant, R.L. Willis, Preparation and characterisation of novel thick sol-gel titania film photocatalysts, Photochem. Photobiol. Sci. 2 (2003) 591–596.

[50] C. Liang, C.-F. Huang, N. Mohanty, R.M. Kurakalva, A rapid spectrophotometric determination of persulfate anion in ISCO, Chemosphere 73 (2008) 1540–1543.

[51] K. Santhi, M. Navaneethan, S. Harish, S. Ponnusamy, C. Muthamizhchelvan, Synthesis and characterization of TiO_2 nanorods by hydrothermal method with different pH conditions and their photocatalytic activity, Appl. Surf. Sci. 500 (2020), 144058.

[52] A.A. Shafe, M.D. Hossain, R.A. Mayanovic, V. Roddatis, M. Benamara, Tuning exchange coupling in NiO-based bimagnetic heterostructured nanocrystals, ACS Appl. Mater. Interfaces 13 (2021) 24013–24023.

[53] P. Taneja, S. Sharma, A. Umar, S.K. Mehta, A.O. Ibhadon, S.K. Kansal, Visible-light driven photocatalytic degradation of brilliant green dye based on cobalt tungstate ($CoWO_4$) nanoparticles, Mater. Chem. Phys. 211 (2018) 335–342.

[54] Z. Zhang, X. Hao, S. Hao, X. Yu, Y. Wang, J. Li, Preparation of 2D WO_3 nanomaterials and their catalytic performance during the synthesis of imines under visible light irradiation, Mol. Catal. 503 (2021), 111427.

[55] D. Nagy, T. Firkala, E. Drotár, Á. Szegedi, K. László, I.M. Szilágyi, Photocatalytic WO_3/TiO_2 nanowires: WO_3 polymorphs influencing the atomic layer deposition of TiO_2, RSC Adv. 6 (2016) 95369–95377.

[56] X. Gao, J. Fei, Y. Dai, F. Fu, Hydrothermal synthesis of series Cu-doped Bi_2WO_6 and its application in photo-degradative removal of phenol in wastewater with enhanced efficiency, J. Mol. Liq. 256 (2018) 267–276.

[57] K.G.N. Quiton, Y.-H. Huang, M.-C. Lu, Recovery of cobalt and copper from single- and co-contaminated simulated electroplating wastewater via carbonate and hydroxide precipitation, Sustain. Environ. Res. 32 (2022) 31.

[58] L. Yang, Y. Wang, Y. Wang, X. Wang, L. Wang, G. Han, Shape-controlled synthesis of $MnWO_4$ nanocrystals via a simple hydrothermal method, J. Alloy. Compd. 578 (2013) 215–219.

[59] Y. Sun, Y. Xia, Shape-controlled synthesis of gold and silver nanoparticles, Science 298 (2002) 2176–2179.

[60] J. Zhao, Y. Zhang, X. Quan, S. Chen, Enhanced oxidation of 4-chlorophenol using sulfate radicals generated from zero-valent iron and peroxydisulfate at ambient temperature, Sep. Purif. Technol. 71 (2010) 302–307.

[61] Y.-Y. Ahn, E.-T. Yun, J.-W. Seo, C. Lee, S.H. Kim, J.-H. Kim, J. Lee, Activation of peroxymonosulfate by surface-loaded noble metal nanoparticles for oxidative degradation of organic compounds, Environ. Sci. Technol. 50 (2016) 10187–10197.

[62] J. Liang, M. Guo, Y. Xue, J.-n. Gu, J. Li, F. Shi, X. Guo, X. Min, J. Jia, K. Li, T. Sun, Constructing magnetically separable manganese-based spinel ferrite from spent ternary lithium-ion batteries for efficient degradation of bisphenol A via peroxymonosulfate activation, Chem. Eng. J. 435 (2022), 135000.

[63] Q. Hu, J. Cao, Z. Yang, W. Xiong, Z. Xu, P. Song, M. Jia, Y. Zhang, H. Peng, A. Wu, Fabrication of Fe-doped cobalt zeolitic imidazolate framework derived from Co $(OH)_2$ for degradation of tetracycline via peroxymonosulfate activation, Sep. Purif. Technol. 259 (2021), 118059.

[64] A.M. Alkadhem, M.A.A. Elgzoly, S.A. Onaizi, Novel amine-functionalized magnesium oxide adsorbents for CO_2 capture at ambient conditions, J. Environ. Chem. Eng. 8 (2020), 103968.

[65] L.M. Darabian, G.R. Gonçalves, M.A. Schettino, E.C. Passamani, J.C.C. Freitas, Synthesis of nanostructured iron oxides and study of the thermal crystallization process using DSC and in situ XRD experiments, Mater. Chem. Phys. 285 (2022), 126065.

[66] T.H. Jeon, H.-i. Cho, H. Park, H.-i. Kim, W. Choi, Synergistic effect of Sn doping and hydrogenation on hematite electrodes for photoelectrochemical water oxidation, Mat. Chem. Front. 5 (2021) 6592–6602.

[67] M.S. Koo, H. Kim, K.E. Lee, W. Choi, Photoconversion of cyanide to dinitrogen using the durable electrode of a TaON overlayer-deposited WO_3 film and visible light, ACS EST Eng. 1 (2021) 228–238.

[68] X. Xu, Y. Feng, Z. Chen, S. Wang, G. Wu, T. Huang, J. Ma, G. Wen, Activation of peroxymonosulfate by $CuCo_2O_4$-GO for efficient degradation of bisphenol A from aqueous environment, Sep. Purif. Technol. 251 (2020), 117351.

[69] F. Wang, M. Xiao, X. Ma, S. Wu, M. Ge, X. Yu, Insights into the transformations of Mn species for peroxymonosulfate activation by tuning the Mn_3O_4 shapes, Chem. Eng. J. 404 (2021), 127097.

[70] A. Khan, Z. Liao, Y. Liu, A. Jawad, J. Ifthikar, Z. Chen, Synergistic degradation of phenols using peroxymonosulfate activated by CuO-Co_3O_4@MnO_2 nanocatalyst, J. Hazard. Mater. 329 (2017) 262–271.

[71] W. Qu, H. Wen, X. Qu, Y. Guo, L. Hu, W. Liu, S. Tian, C. He, D. Shu, Enhanced Fenton-like catalysis for pollutants removal via MOF-derived $Co_xFe_{3-x}O_4$ membrane: oxygen vacancy-mediated mechanism, Chemosphere 303 (2022), 135301.

[72] L. Wu, P. Guo, X. Wang, H. Li, A. Li, K. Chen, Mechanism study of CoS_2/Fe(III)/peroxymonosulfate catalysis system: the vital role of sulfur vacancies, Chemosphere 288 (2022), 132646.
[73] Q. Deng, X. Zhang, L. Chang, H. Chai, Y. Huang, The MOF/LDH derived heterostructured Co_3O_4/$MnCo_2O_4$ composite for enhanced degradation of levofloxacin by peroxymonosulfate activation, Sep. Purif. Technol. 294 (2022), 121182.
[74] J. Wang, R. Peng, K. Chen, Y. Wang, T. Xie, Q. Zhu, Y. Peng, S. Liu, Z. Yao, A novel $CoNi_7O_8$/MnO_2 nanocomposite supported on Ni foam as a peroxymonosulfate activator for the highly efficient singlet oxygen mediated removal of methylene blue, New J. Chem. 46 (2022) 7569–7579.
[75] Q. Ma, Y. Zhang, X. Zhu, B. Chen, Hollow multi-shelled Co_3O_4 as nanoreactors to activate peroxymonosulfate for highly effective degradation of Carbamazepine: a novel strategy to reduce nano-catalyst agglomeration, J. Hazard. Mater. 427 (2022), 127890.
[76] J. Yu, W. Qiu, H. Xu, X. Lu, J. Ma, D. Lu, Highly-efficient and stable $MgCo_2O_4$ spinel for bisphenol a removal by activating peroxymonosulfate via radical and non-radical pathways, Chem. Eng. J. 421 (2021), 129498.
[77] J. Hu, X. Zeng, Y. Yin, Y. Liu, Y. Li, X. Hu, L. Zhang, X. Zhang, Accelerated alkaline activation of peroxydisulfate by reduced rubidium tungstate nanorods for enhanced degradation of bisphenol A, Environ. Sci. Nano 7 (2020) 3547–3556.
[78] R.H.D. dos Passos, C.P. de Souza, C. Bernard-Nicod, C. Leroux, M. Arab, Structural and electrical properties of cerium tungstate: application to methane conversion, Ceram. Int. 46 (2020) 8021–8030.
[79] J. Zhao, F. Li, H. Wei, H. Ai, L. Gu, J. Chen, L. Zhang, M. Chi, J. Zhai, Superior performance of $ZnCoO_x$/peroxymonosulfate system for organic pollutants removal by enhancing singlet oxygen generation: the effect of oxygen vacancies, Chem. Eng. J. 409 (2021), 128150.
[80] X. Long, C. Feng, D. Ding, N. Chen, S. Yang, H. Chen, X. Wang, R. Chen, Oxygen vacancies-enriched $CoFe_2O_4$ for peroxymonosulfate activation: the reactivity between radical-nonradical coupling way and bisphenol A, J. Hazard. Mater. 418 (2021), 126357.
[81] Z. Wang, Z. Wang, W. Li, Y. Lan, C. Chen, Performance comparison and mechanism investigation of Co_3O_4-modified different crystallographic MnO_2 (α, β, γ, and δ) as an activator of peroxymonosulfate (PMS) for sulfisoxazole degradation, Chem. Eng. J. 427 (2022), 130888.
[82] J. Xu, Y. Wang, J. Wan, L. Wang, Facile synthesis of carbon-doped $CoMn_2O_4$/Mn_3O_4 composite catalyst to activate peroxymonosulfate for ciprofloxacin degradation, Sep. Purif. Technol. 287 (2022), 120576.
[83] G.V. Buxton, C.L. Greenstock, W.P. Helman, A.B. Ross, Critical review of rate constants for reactions of hydrated electrons, hydrogen atoms and hydroxyl radicals (•OH/•O^-) in aqueous solution, J. Phys. Chem. Ref. Data 17 (1988) 513–886.
[84] P. Neta, R.E. Huie, A.B. Ross, Rate constants for reactions of inorganic radicals in aqueous solution, J. Phys. Chem. Ref. Data 17 (1988) 1027–1284.
[85] C. Li, J. Wu, W. Peng, Z. Fang, J. Liu, Peroxymonosulfate activation for efficient sulfamethoxazole degradation by Fe_3O_4/β-FeOOH nanocomposites: coexistence of radical and non-radical reactions, Chem. Eng. J. 356 (2019) 904–914.
[86] H. Chen, Y. Xu, K. Zhu, H. Zhang, Understanding oxygen-deficient $La_2CuO_{4-\delta}$ perovskite activated peroxymonosulfate for bisphenol A degradation: the role of localized electron within oxygen vacancy, Appl. Catal. B Environ. 284 (2021), 119732.
[87] A.A. Gorman, M.A.J. Rodgers, Singlet molecular oxygen, Chem. Soc. Rev. 10 (1981) 205–231.
[88] X. Li, Z. Zhao, H. Li, J. Qian, Degradation of organic contaminants in the $CoFe_2O_4$/peroxymonosulfate process: the overlooked role of Co(II)-PMS complex, Chem. Eng. J. Adv. 8 (2021), 100143.
[89] L. Wang, J. Jiang, S.-Y. Pang, Y. Zhou, J. Li, S. Sun, Y. Gao, C. Jiang, Oxidation of bisphenol A by nonradical activation of peroxymonosulfate in the presence of amorphous manganese dioxide, Chem. Eng. J. 352 (2018) 1004–1013.
[90] W. Tan, W. Ren, C. Wang, Y. Fan, B. Deng, H. Lin, H. Zhang, Peroxymonosulfate activated with waste battery-based Mn-Fe oxides for pollutant removal: electron transfer mechanism, selective oxidation and LFER analysis, Chem. Eng. J. 394 (2020), 124864.
[91] A. Ahmed, M. Usman, B. Yu, F. Gao, Y. Shen, H. Cong, Heterogeneous activation of peroxymonosulfate using superparamagnetic β-CD-$CoFe_2O_4$ catalyst for the removal of endocrine-disrupting bisphenol A: performance and degradation mechanism, Sep. Purif. Technol. 279 (2021), 119752.
[92] S. Fadaei, M. Noorisepehr, H. Pourzamani, M. Salari, M. Moradnia, M. Darvishmotevalli, N. Mengelizadeh, Heterogeneous activation of peroxymonosulfate with Fe_3O_4 magnetic nanoparticles for degradation of Reactive Black 5: batch and column study, J. Environ. Chem. Eng. 9 (2021), 105414.
[93] S.B. Hammouda, F. Zhao, Z. Safaei, D.L. Ramasamy, B. Doshi, M. Sillanpää, Sulfate radical-mediated degradation and mineralization of bisphenol F in neutral medium by the novel magnetic Sr_2CoFeO_6 double perovskite oxide catalyzed peroxymonosulfate: influence of co-existing chemicals and UV irradiation, Appl. Catal. B Environ. 233 (2018) 99–111.
[94] Y. Wang, D. Tian, W. Chu, M. Li, X. Lu, Nanoscaled magnetic $CuFe_2O_4$ as an activator of peroxymonosulfate for the degradation of antibiotics norfloxacin, Sep. Purif. Technol. 212 (2019) 536–544.
[95] J. Li, Y. Wan, Y. Li, G. Yao, B. Lai, Surface Fe(III)/Fe(II) cycle promoted the degradation of atrazine by peroxymonosulfate activation in the presence of hydroxylamine, Appl. Catal. B Environ. 256 (2019), 117782.
[96] H. Zheng, J. Bao, Y. Huang, L. Xiang, M. Faheem, B. Ren, J. Du, M.N. Nadagouda, D.D. Dionysiou, Efficient degradation of atrazine with porous sulfurized Fe_2O_3 as catalyst for peroxymonosulfate activation, Appl. Catal. B Environ. 259 (2019), 118056.
[97] K. Kim, N.T.H. Le, A.Q.K. Nguyen, Y.-Y. Ahn, B. Kim, G. Shin, W. Choi, J. Kim, Freezing-induced activation of the binary chloride-Oxone system to free chlorine and its application in water treatment, Chem. Eng. J. 428 (2022), 131134.
[98] D.T. Oyekunle, E.A. Gendy, J. Ifthikar, Z. Chen, Heterogeneous activation of persulfate by metal and non-metal catalyst for the degradation of sulfamethoxazole: a review, Chem. Eng. J. 437 (2022), 135277.
[99] B.C. Hodges, E.L. Cates, J.-H. Kim, Challenges and prospects of advanced oxidation water treatment processes using catalytic nanomaterials, Nat. Nanotechnol. 13 (2018) 642–650.